



**HAL**  
open science

## Monitoring of stable isotope composition of precipitation reveals thunderstorm dynamics

Ana-Voica Bojar, Christophe Lécuyer, Hans-Peter Bojar, François Fourel,  
Stanislaw Chmiel

► **To cite this version:**

Ana-Voica Bojar, Christophe Lécuyer, Hans-Peter Bojar, François Fourel, Stanislaw Chmiel. Monitoring of stable isotope composition of precipitation reveals thunderstorm dynamics. *Isotopes in Environmental and Health Studies*, 2024, pp.1-16. 10.1080/10256016.2024.2380059 . hal-04885531

**HAL Id: hal-04885531**

**<https://hal.science/hal-04885531v1>**

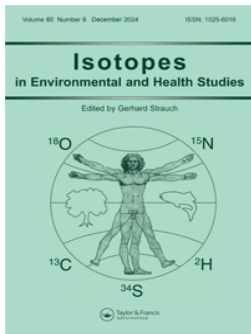
Submitted on 16 Jan 2025

**HAL** is a multi-disciplinary open access archive for the deposit and dissemination of scientific research documents, whether they are published or not. The documents may come from teaching and research institutions in France or abroad, or from public or private research centers.

L'archive ouverte pluridisciplinaire **HAL**, est destinée au dépôt et à la diffusion de documents scientifiques de niveau recherche, publiés ou non, émanant des établissements d'enseignement et de recherche français ou étrangers, des laboratoires publics ou privés.



Distributed under a Creative Commons Attribution - NonCommercial - NoDerivatives 4.0  
International License



## Monitoring of stable isotope composition of precipitation reveals thunderstorm dynamics

Ana-Voica Bojar, Christophe Lécuyer, Hans-Peter Bojar, François Fourel & Stanislaw Chmiel

To cite this article: Ana-Voica Bojar, Christophe Lécuyer, Hans-Peter Bojar, François Fourel & Stanislaw Chmiel (27 Jul 2024): Monitoring of stable isotope composition of precipitation reveals thunderstorm dynamics, *Isotopes in Environmental and Health Studies*, DOI: [10.1080/10256016.2024.2380059](https://doi.org/10.1080/10256016.2024.2380059)

To link to this article: <https://doi.org/10.1080/10256016.2024.2380059>



© 2024 The Author(s). Published by Informa UK Limited, trading as Taylor & Francis Group



Published online: 27 Jul 2024.



Submit your article to this journal [↗](#)



Article views: 367




View related articles [↗](#)



View Crossmark data [↗](#)

## Monitoring of stable isotope composition of precipitation reveals thunderstorm dynamics

Ana-Voica Bojar <sup>a,b</sup>, Christophe Lécuyer<sup>c,d</sup>, Hans-Peter Bojar<sup>b</sup>, François Fourel<sup>e</sup> and Stanislaw Chmiel<sup>f</sup>

<sup>a</sup>Department of Geology, Salzburg University, Salzburg, Austria; <sup>b</sup>Department of Mineralogy, Universalmuseum Joanneum, Graz, Austria; <sup>c</sup>Laboratoire de Géologie de Lyon, CNRS UMR 5276, Université Claude Bernard Lyon 1, Villeurbanne, France; <sup>d</sup>Institut Universitaire de France, Paris, France; <sup>e</sup>Laboratoire d'Ecologie des Hydrosystèmes Naturels et Anthropisés, LEHNA UMR CNRS 5023, Université Claude Bernard Lyon 1, Villeurbanne, France; <sup>f</sup>Faculty of Earth Sciences and Spatial Management, Maria Curie-Skłodowska University, Lublin, Poland

### ABSTRACT

The summer of 2019 is particularly well known for the famous heatwaves that swept across the European continent, with its associated drought and record-breaking air temperatures. This was followed by powerful thunderstorms, characterised by hail and heavy rain that damaged the crops on a regional scale. Here, we investigated one of the largest storm cells, lasting more than 6 h, which struck southwestern Romania. High-temporal resolution sampling of storm precipitation was performed for stable isotope measurements, rainfall and air temperature, to follow the storm dynamics. Hydrogen and oxygen isotope measurements show an abrupt decreasing temporal trend followed by superimposed V-shaped patterns interpreted as reflecting moisture replenishment by successive rain bands. To model the stable isotope values of precipitation in relation to the general trend of decreasing air temperatures, we applied a numerical Rayleigh condensation model for a non-constant  $\alpha$  isotopic fractionation factor between liquid water and water vapour. The storm is powered by four consecutive moisture fronts, each following a Rayleigh distribution. About 40 % of the water vapour condenses during the sampled storm due to adiabatic expansion and cooling, which lowers saturation. Condensation ceases when cooling and absolute humidity can no longer sustain the dew point, stopping the rain. The timing of the event, occurring late at night and early in the morning, its duration of over 6 h as well as its synoptic scale may indicate a mesoscale convective complex.

### ARTICLE HISTORY

Received 21 September 2023  
Accepted 25 June 2024

### KEYWORDS

Heat wave; storm cell; stable isotopes; moisture replenishment; Rayleigh condensation; South Carpathian Hills; Water sources; fractionation at variable temperature

**CONTACT** Ana-Voica Bojar  ana-voica.bojar@plus.ac.at  Department of Geology, Salzburg University, Hellbrunnerstrasse 34, Salzburg A-5020, Austria

This article has been corrected with minor changes. These changes do not impact the academic content of the article.  
**We would like to dedicate this paper to Stanislaw Hałas (1945–2017), Marie Curie-Skłodowska University, Lublin, Poland, for his inspiring presence in the field of isotope geochemistry.**

© 2024 The Author(s). Published by Informa UK Limited, trading as Taylor & Francis Group  
This is an Open Access article distributed under the terms of the Creative Commons Attribution-NonCommercial-NoDerivatives License (<http://creativecommons.org/licenses/by-nc-nd/4.0/>), which permits non-commercial re-use, distribution, and reproduction in any medium, provided the original work is properly cited, and is not altered, transformed, or built upon in any way. The terms on which this article has been published allow the posting of the Accepted Manuscript in a repository by the author(s) or with their consent.

## 1. Introduction

In southwestern Romania, including Mehedinți County, water sources are limited to springs and recently drilled wells that tap into Quaternary clastic deposits [1]. In their study, Bojar et al. [2] determined the local meteoric water line (LMWL) (Figure 1A), the seasonal variations of precipitation  $\delta^{18}\text{O}$  and  $\delta^2\text{H}$  values, the deuterium excess, and the monthly  $T$ - $\delta^{18}\text{O}$  relationship. Another study conducted by Bojar et al. [3] investigated the compositions of cationic and anionic groundwater of approximately 30 springs and wells, their distribution along local geological structures, and the water age using the  $^{14}\text{C}$  method. The results provide a comprehensive picture of aquifers, spring distribution,

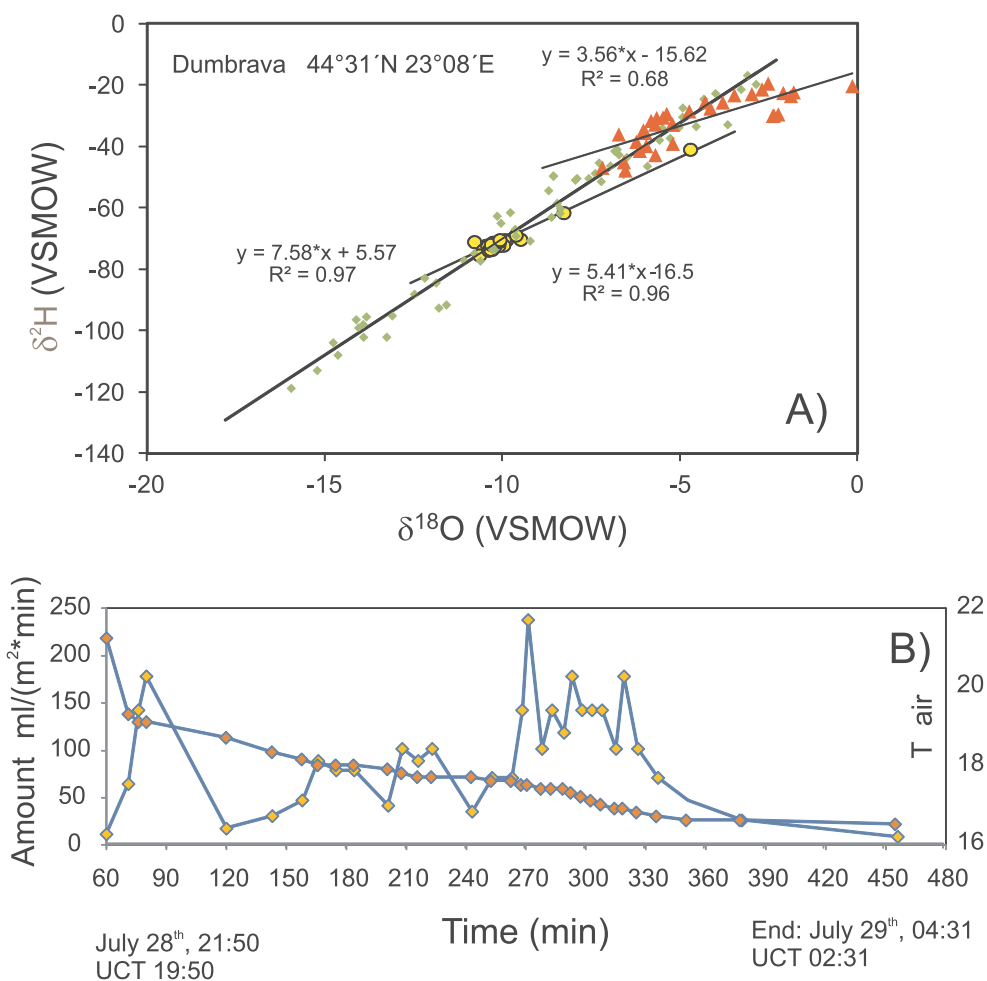


**Figure 1.** A. Biplot of oxygen and hydrogen isotope compositions of storm rainfall samples and the local meteoric water line (LMWL) and evaporation lines. The green points define the LMWL, the yellow points are the isotopic composition of springs and lake defining the LEL, the red triangles define the line for the investigated storm, line intersecting the LMWL. B. Precipitation amount collected during storm (yellow diamonds) is given in  $\text{ml}/(\text{m}^2 \cdot \text{min})$ . Measured air temperature in  $^{\circ}\text{C}$  (orange diamonds) with time plotted on the x-axis. For the start and the end of the x-scale representing the duration of storm, UCT and local time (+2 h) are used. Between the start and end of the record, measured time is given in minutes.

and water chemistry. In the study area, the only source of aquifer recharge and water for crops and the population are summer to early autumn storms (June to September). The area experiences a minimum amount of rainfall during summer and early autumn. The presence of summer precipitation events is crucial for the entire region.

July 2019 is known as the hottest month on record in Europe, with a pronounced heat wave occurring between 20 and 28 July. The heat wave was caused by a block of hot, dry air from North Africa that was trapped between cold storm systems. This high pressure area stretched from the central Mediterranean to Scandinavia and was delimited by low pressure areas over western Russia and the eastern Atlantic, resulting in drought and extreme temperatures across Europe. ([www.eumetsat.int/european-heatwaves-summer-2019](http://www.eumetsat.int/european-heatwaves-summer-2019); [public.wmo.int/en/media/news/july-matched-and-maybe-broke-record-hottest-month-analysis-began](http://public.wmo.int/en/media/news/july-matched-and-maybe-broke-record-hottest-month-analysis-began); [surfobs.climate.copernicus.eu/stateoftheclimate/june2019.php](http://surfobs.climate.copernicus.eu/stateoftheclimate/june2019.php); [www.worldweatherattribution.org/human-contribution-to-the-record-breaking-july-2019-heat-wave-in-western-europe](http://www.worldweatherattribution.org/human-contribution-to-the-record-breaking-july-2019-heat-wave-in-western-europe); [en.wikipedia.org/wiki/2019\\_European\\_heat\\_waves](https://en.wikipedia.org/wiki/2019_European_heat_waves); last accessed March 31, 2023). The heat wave was broken by severe storms including also hail, which wiped out crops regionally ([www.dw.com/en/europe-lashed-by-hail-fatal-storms/a-49778989](http://www.dw.com/en/europe-lashed-by-hail-fatal-storms/a-49778989)).

The study area, located in the south-western part of the Carpathians, experienced a July heat wave that was interrupted by an unusually long storm from 19:00 UCT on 28 July–03:00 UCT on 29 July (+2 h for the local time). The study is based on detailed time series of temperature distribution, rainfall intensity, and stable isotope data measured during this storm. To explain the observed distributions, the data acquired were modelled and linked to available meteorological information, proposing a mechanism for storm development. The records provide quantitative insights into the event and evaluate the impact of a severe storm in a region with temperature variations of over 25 °C between winter and summer, and a high continentality index [2], which measures the range between minimum and maximum yearly air temperatures, reflecting the relative influence of oceanic masses inland.

The aim of this study is to investigate how the stable isotope composition of rainwater changes over time during a large storm event. This can provide insights into the dynamics of rain formation and the processes influencing isotopic fractionation. Understanding how the stable isotope composition of rainwater evolves during a storm event can also have important implications for hydrological processes, including groundwater recharge, surface runoff, and water resource management. Furthermore, the analysis of stable isotopes in rainwater during extreme precipitation events can help in evaluating the effects of climate change on precipitation patterns.

## 2. Methods and materials

### 2.1. Precipitation sampling

For this study, 33 samples were collected continuously during the night of 28–29 July 2019 in the Mehedinți district, south of the South Carpathians at an altitude of 350 m above the sea level. Sequential sampling of rainwater was carried out using an apparatus similar to that of Bourrié [4]. The rain collector had an area of 421 cm<sup>2</sup> and fed through a pipe a series of glass bottles that were filled in sequence. The duration required to fill a 150 ml bottle was measured using a chronometer, thus the time measured in order to collect each sample may vary depending on the rain intensity. Air temperatures were measured every 30 min

with a data logger and the results interpolated over the sampling time (Figure 1B, Figure 3, Figure 4). A total of 990 ml of rainwater was collected over a period of 456 min.

## 2.2. Stable isotope measurements

Hydrogen isotope measurements were performed using the chromium-based reduction technique described in [5]. For the isotopic measurements of each water sample, the  $\delta^2\text{H}$  (‰ VSMOW) corresponds to the average of five aliquots of 0.5  $\mu\text{L}$  collected from the same sample. The method is based on water reduction using a chromium-based reactor installed in a EuroEA3028-HT<sup>TM</sup> elemental analyser from Eurovector SpA (Milan, Italy). This elemental analyser has been upgraded with a EuroAS300 series liquid autosampler equipped with a 1- $\mu\text{L}$  1BR-5 SGE syringe. The elemental analyser is connected online in continuous flow mode to an IsoPrime Isotopic Ratio Mass Spectrometer from IsoPrime UK Ltd (Cheadle, UK). The mass spectrometer is equipped with an electrostatic filter to prevent helium interferences on hydrogen mass 3 beams. The  $\text{H}_3^+$  factor was calculated daily and was usually less than 10 ppm/nA. The duration of each analytical run is approximately 300 s. Water samples collected from the vacuum line were pipetted into 13  $\times$  32 mm vials with butyl/Teflon sealed caps. If the volume of water collected from

**Table 1.** Isotopic composition of the serial water samples collected during the storm event. Standard deviation (SD) is given at  $\pm 1 \sigma$ .

Sample#	$\delta^{18}\text{O}$ (‰ VSMOW)	SD (n = 4)	$\delta^2\text{H}$ (‰ VSMOW)	SD
AV1	-0.13	0.07	-20.33	0.52
AV2	-2.21	0.10	-29.54	0.84
AV3	-2.37	0.04	-30.05	0.41
AV4	-2.34	0.09	-29.87	0.39
AV5	-1.86	0.07	-23.57	0.69
AV6	-1.78	0.07	-22.36	0.85
AV7	-2.07	0.04	-22.56	0.42
AV8	-2.96	0.05	-22.97	0.51
AV9	-2.50	0.05	-19.50	0.61
AV10	-2.67	0.03	-21.42	0.53
AV11	-3.45	0.12	-23.31	0.36
AV12	-3.78	0.08	-25.66	0.41
AV13	-4.13	0.05	-27.63	0.53
AV14	-4.72	0.02	-28.56	0.50
AV15	-4.27	0.00	-25.62	0.56
AV16	-5.19	0.09	-32.94	0.40
AV17	-5.20	0.05	-32.73	0.41
AV18	-5.68	0.10	-32.86	0.29
AV19	-5.80	0.01	-31.66	0.39
AV20	-5.36	0.04	-29.38	0.32
AV21	-5.46	0.04	-30.57	0.30
AV22	-5.64	0.04	-30.73	0.56
AV23	-6.01	0.04	-34.74	0.38
AV24	-5.95	0.12	-35.60	0.49
AV25	-6.71	0.09	-36.08	0.72
AV26	-6.21	0.04	-38.49	0.34
AV27	-5.93	0.03	-39.86	0.41
AV28	-6.12	0.12	-41.42	0.37
AV29	-6.56	0.06	-45.15	0.41
AV30	-6.52	0.01	-47.81	0.35
AV31	-7.17	0.10	-46.94	0.45
AV32	-5.68	0.09	-42.79	0.15
AV33	-5.18	0.11	-39.12	0.65

the sublimation experiment was too small, special inserts had to be placed in the vials to meet the specifications of the liquid autosampler. Five injections were made from each vial of water, from which the standard deviations ( $2\sigma$ ) reported in Table 1 were calculated. Hydrogen isotope ratios are reported relative to VSMOW in the ‰  $\delta$  unit, after scaling the raw data to the certified isotopic ratios of VSMOW2 and VSLAP2 [6,7] to which we also added aliquots of GISP former international standard [8–11].

The  $^{18}\text{O}/^{16}\text{O}$  analyses from water samples were carried out using an isoFLOW system in water equilibration mode [12–14] connected on line in continuous flow mode to a precision mass spectrometer operated by a Vision software from Elementar Uk Ltd. 200  $\mu\text{L}$  aliquots were loaded in LABCO Exetainer® 3.7-ml soda glass vials, round bottomed, non-evacuated. The sample vial headspace was automatically flushed with helium with the isoFLOW double needle setup. The equilibration gas was a mixture of 10 %  $\text{CO}_2$  in helium automatically introduced in contact with the sample through the isoFLOW. The equilibration reaction took place at 40 °C in a temperature regulated sample tray. The equilibrated  $\text{CO}_2$  gas generated was then transferred to the mass spectrometer via the centrION interface. A calibrated  $\text{CO}_2$  gas was used as a monitoring gas. Calibrated waters were used to anchor the results to the VSLAP/VSMOW scale. The calibrated waters used were EdL III ( $\delta^{18}\text{O}_{\text{VSMOW}} = -9.34$  ‰), EE1 ( $\delta^{18}\text{O}_{\text{VSMOW}} = +6.44$  ‰) and SSRW ( $\delta^{18}\text{O}_{\text{VSMOW}} = -16.0$  ‰). During the course of the experiments the waters used as working standards were calibrated against waters from the WICO intercalibration programme [14]. Aliquots of EdL III were placed at the beginning and at the end of each analytical batch to check for instrumental drift with time. No significant drift was noticed during the experiments. Delta values are expressed with respect to VSMOW. Typical external precision for  $\delta^{18}\text{O}$  analyses from water samples is 0.05 ‰. Samples were systematically duplicated. The isotopic data are displayed in Figures 2–5.

### 2.3. Meteorological data

The data in Figure 6 were obtained from [www.lightningmaps.org/about?lang=de](http://www.lightningmaps.org/about?lang=de) and [www.blitzortung.org/de/historical\\_maps](http://www.blitzortung.org/de/historical_maps) (accessed 27 March 2023).

The temperature distributions in Figure 7 are based on the Hysplit GFS database at 0.25-deg 3S (available from June 13, 2019 DA 2500 Mb). The database records daily files of air temperature every three hours in the native GFS hybrid sigma coordinate system. The data is sourced from NCEP GFS.v15(fv3). The record began on 28 July at 18:00 and ended 24 h later on 29 July. The initial time displayed is offset by two hours from the first database record, and the geographical coordinates are centred on the sampled location in Mehedinți district, specifically 44°31'N and 23°08'E.

### 2.4. Modelling of stable isotope data

#### 2.4.1. Fractionation factor between liquid and vapour

Various fractionation factors have been identified for liquid–vapour exchange, such as those in [15–17]. In this calculation, we have used the equation from Halas [18]:

$$10^3 \ln \alpha_{l-v} = \left( \frac{A \cdot 10^6}{T^2} - \frac{B \cdot 10^3}{T} \right) \left( 1 - e^{-3.3 \left( \frac{T_c - T}{T} \right)} \right) + C \cdot 10^3 \frac{T_c - T}{T^2} e^{-3.3 \left( \frac{T_c - T}{T} \right)} \quad (1)$$

For  $\delta^{18}\text{O}$  the values of parameters are  $A = 1.3781$ ,  $B = 1.8876$ ,  $C = 3.6558$ .

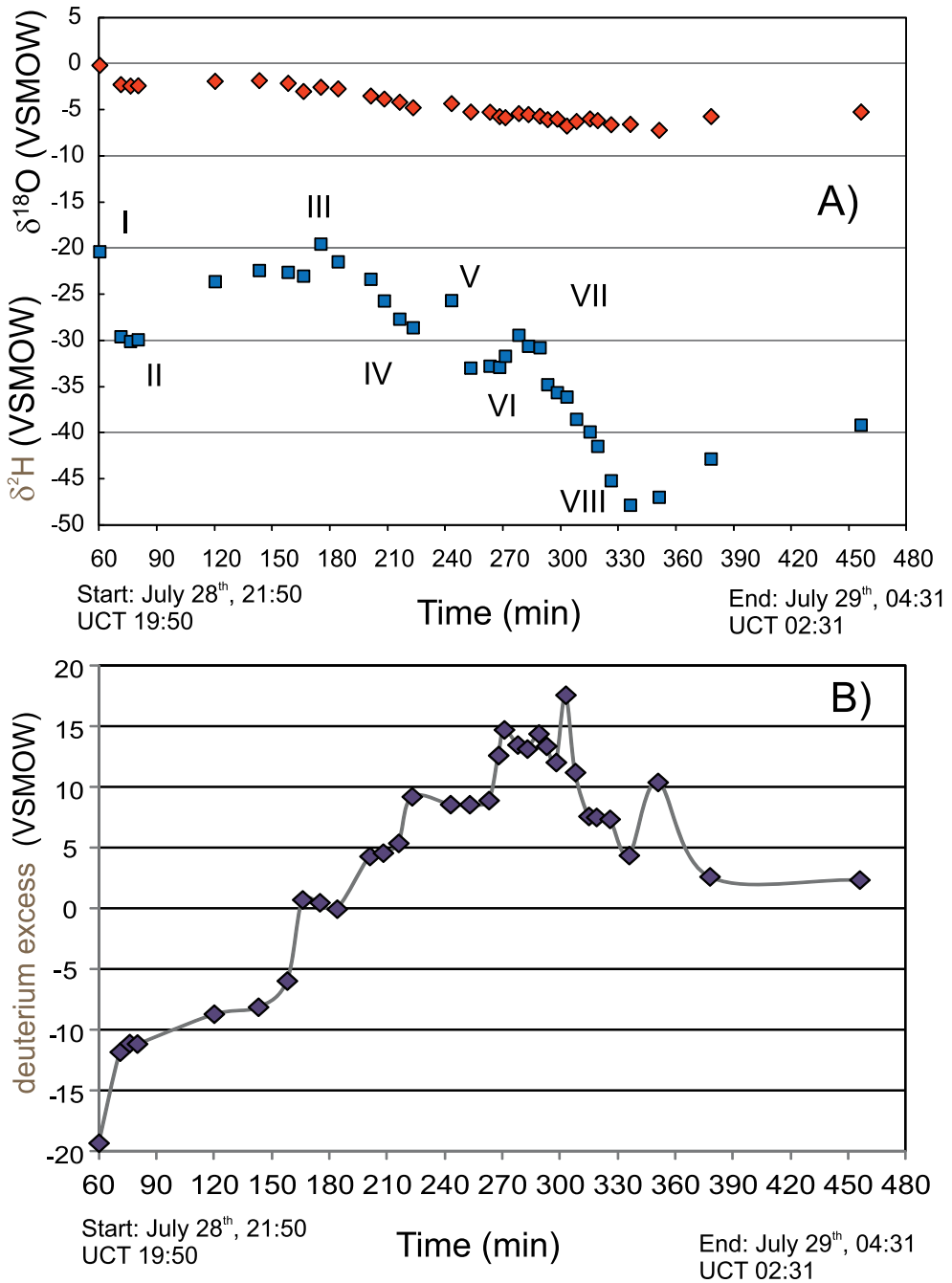


**Figure 2.** A. Variation of oxygen (red) and hydrogen (blue) isotope compositions of rainfall during the storm period; B. Variation of deuterium excess with time.



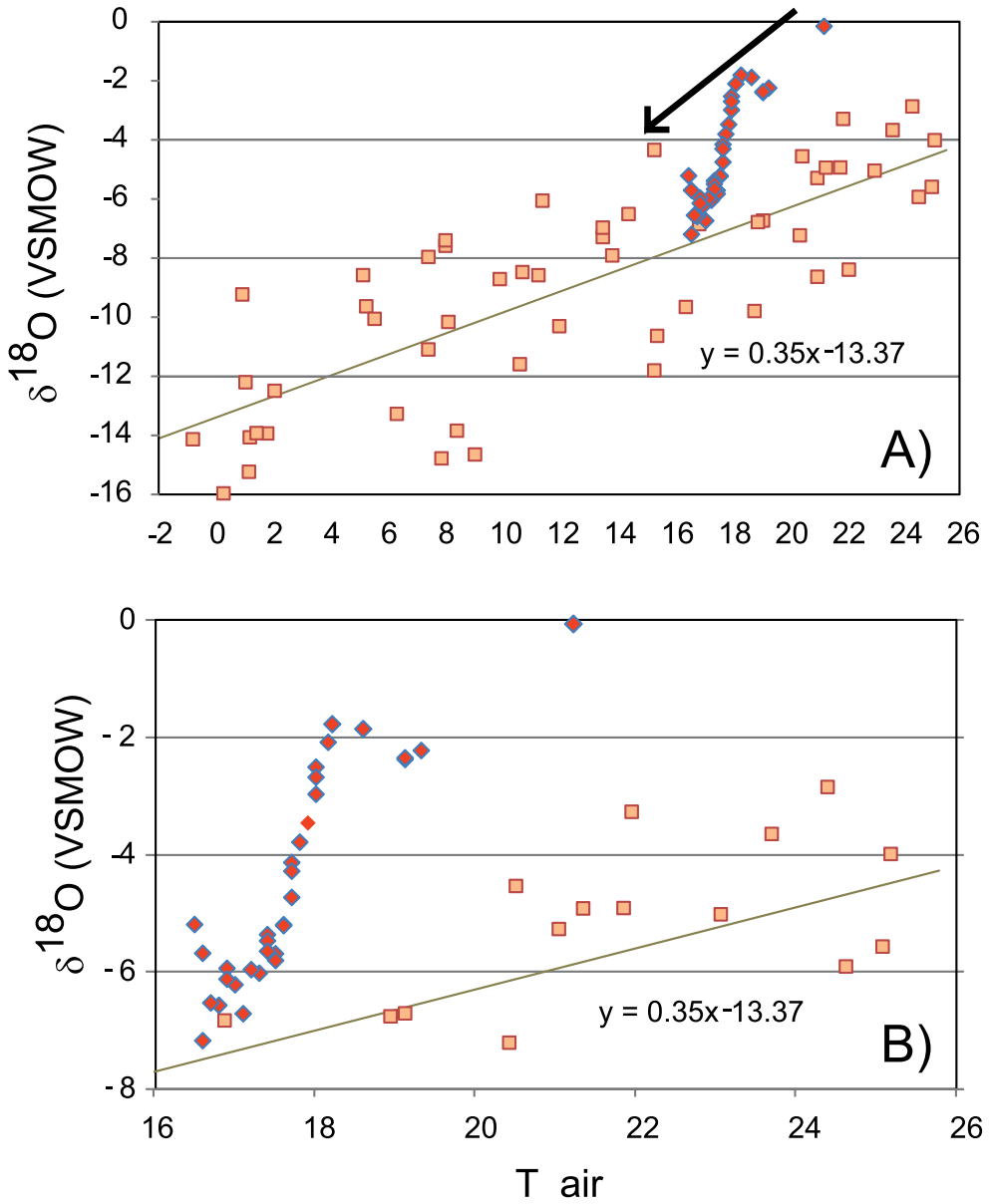


**Figure 3.** A. Variation of the monthly mean  $\delta^{18}O$  values of rain (orange squares) with monthly mean air temperature. The storm rainfall data (red diamonds) are plotting in the summer sector of the biplot. The arrow shows the direction in which values are shifting during storm; B. Zoom for the summer storm sector.

For  $\delta^2H$  the values of parameters are  $A = 18.993$ ,  $B = 40.798$ ,  $C = 18.405$ .

From Equation (1), we can express  $\alpha_{I-v}$  as:

$$\alpha_{I-v} = e^{\left(\frac{A \cdot 10^3}{T^2} - \frac{B}{T}\right) \left(1 - e^{-3.3 \left(\frac{T_c - T}{T}\right)}\right) + C \cdot \frac{T_c - T}{T^2} e^{-3.3 \left(\frac{T_c - T}{T}\right)}} \quad (2)$$

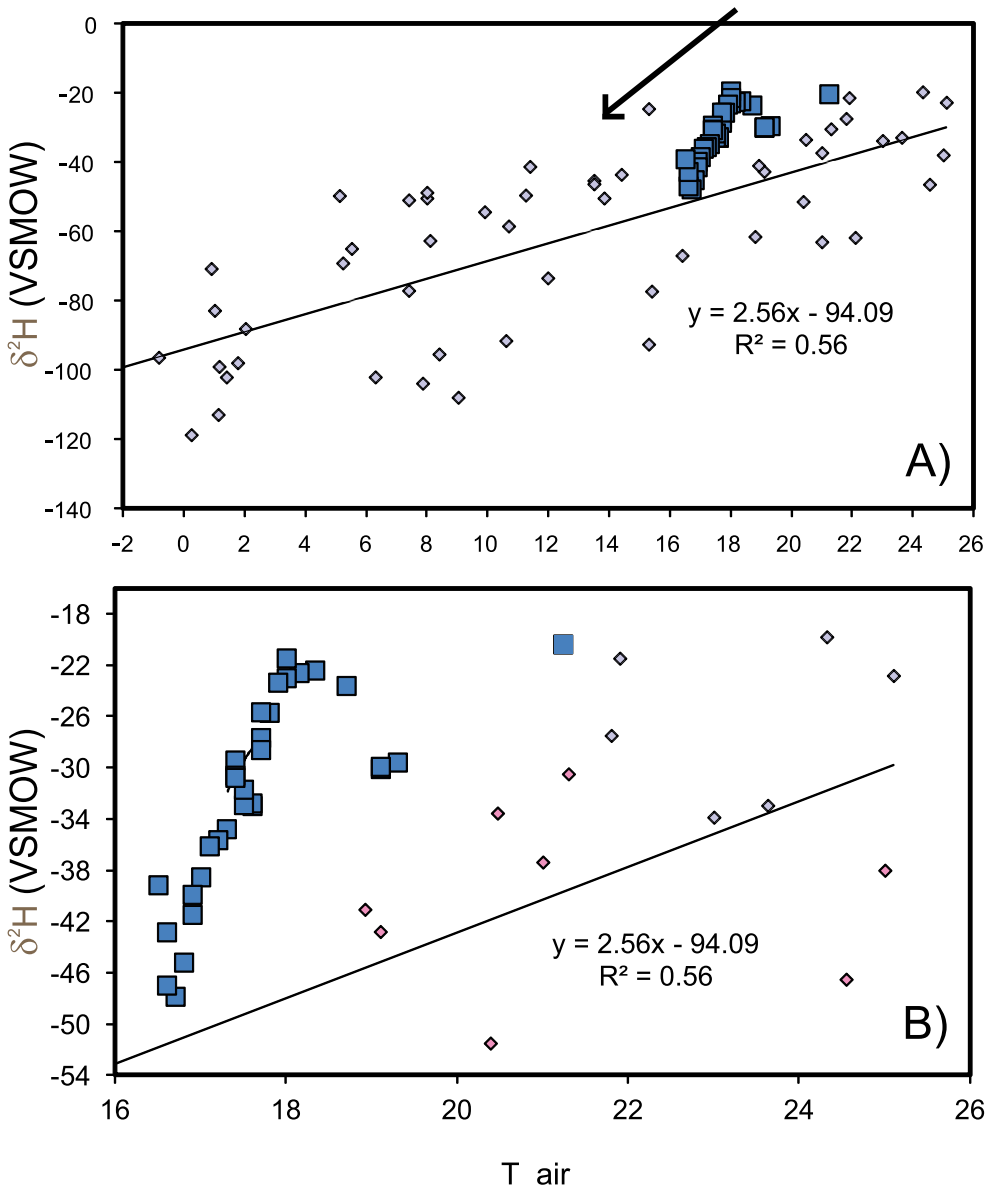


**Figure 4.** A. Variation of the monthly mean  $\delta^2\text{H}$  values of rain (orange squares) with monthly mean air temperature. The storm data (blue squares) are plotting in the summer sector of the biplot. The arrow shows the direction in which values are shifting during storm; B. Zoom for the summer storm sector.

where:  $\alpha_{l-v}$  = fractionation factor between liquid and vapour;  $T$  = temperature in Kelvin;  $T_c$  = critical temperature of water

In this case, the vapour isotopic composition may be calculated as:

$$\delta_v = \frac{1000 + \delta_l}{\alpha_{l-v}} - 1000 \quad (3)$$

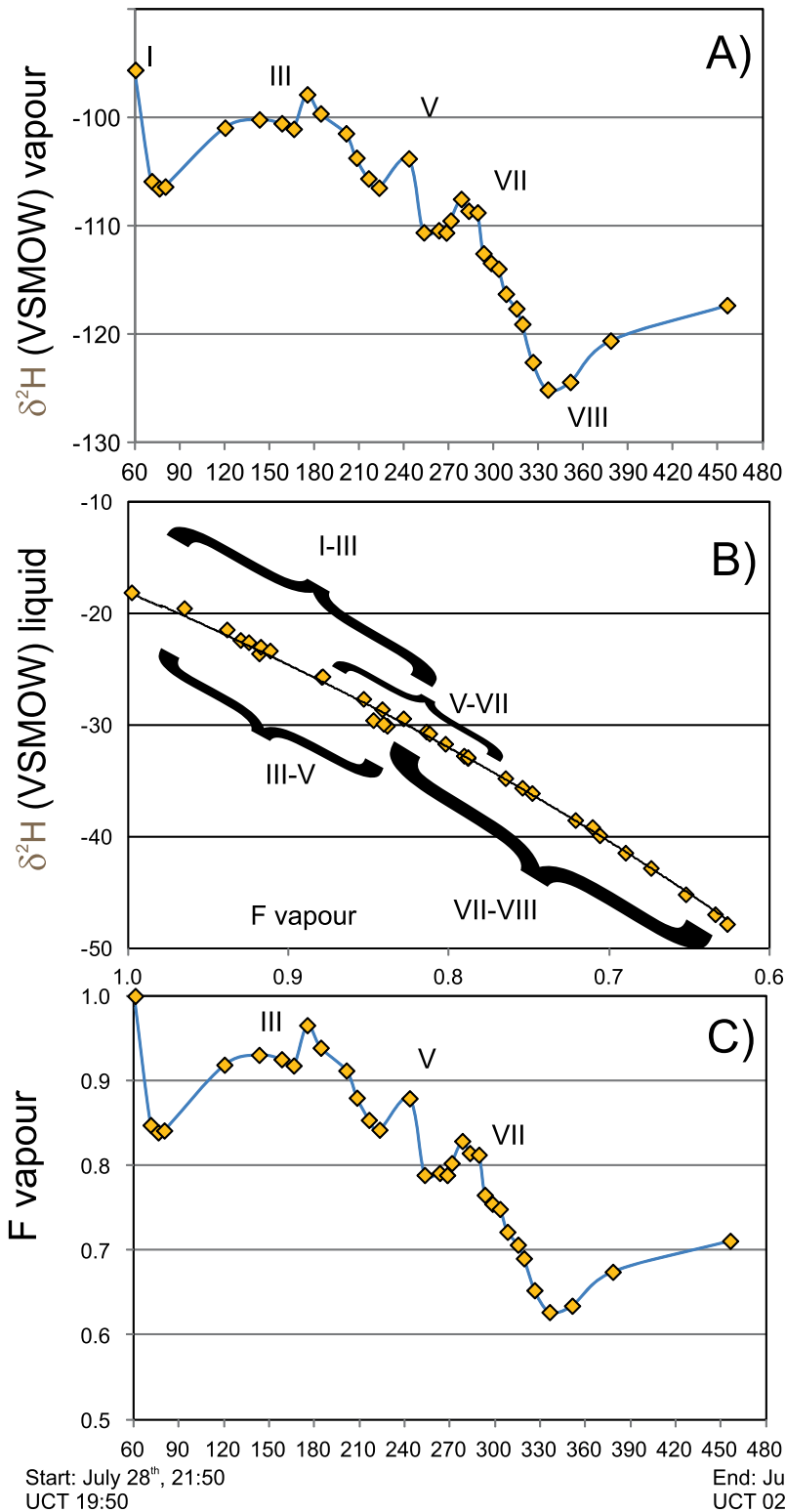


**Figure 5.** A. Rayleigh distillation model for the  $\delta^2\text{H}$  values of rain, F fraction of remaining vapour; B. Variation of F with time, the higher values from III, V, VIII are interpreted as new inputs of vapour fronts.

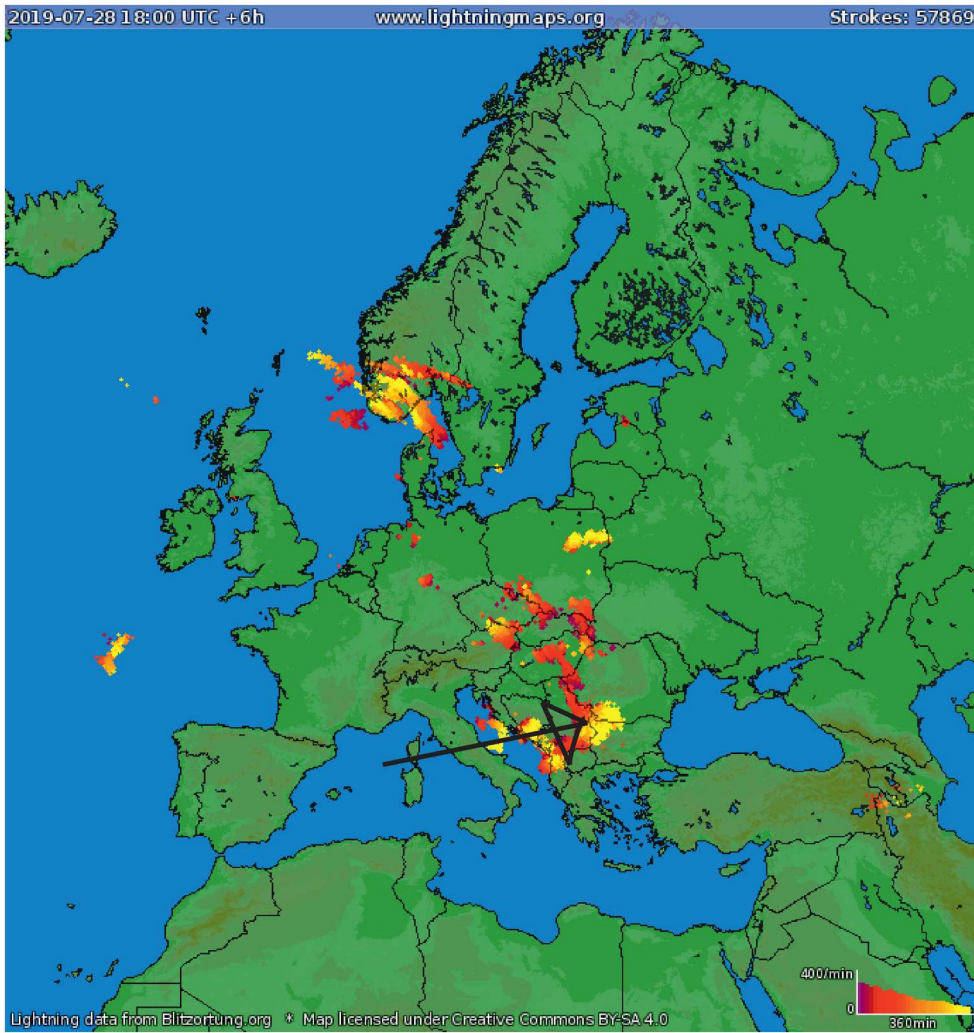


**Figure 6.** Cyclonic Atlantic front striking over the Mediterranean region, the sampling location is pointed with an arrow. The map shows the record of lightnings starting at 18:00 UCT on July 28th and ending at midnight UCT (local time at investigated area 20:00–02:00 on July 29th), ([www.blitzortung.org/de/historical\\_maps](http://www.blitzortung.org/de/historical_maps)).

#### 2.4.2. Rayleigh isotopic fractionation between condensate and vapour at variable temperature

According to [19], the Rayleigh isotopic fractionation between condensate at vapour variable temperature has the expression:

$$\delta_l = \frac{\alpha_{l-v}}{\alpha_0} (\delta_0 + 1000) F^{(\alpha_m - 1)} - 1000 \quad (4)$$

where:  $\delta_l$  = isotopic values for  $\delta^{18}\text{O}$  and  $\delta^2\text{H}$  of condensate liquid;  $\alpha_{l-v}$  = fractionation factor between liquid and vapour;  $\alpha_0$  = fractionation factor at initial temperature  $T_0$ ;  $\alpha_m$  = fractionation factor at temperature  $(T + T_0)/2$ ;  $F$  = fraction of remaining vapour

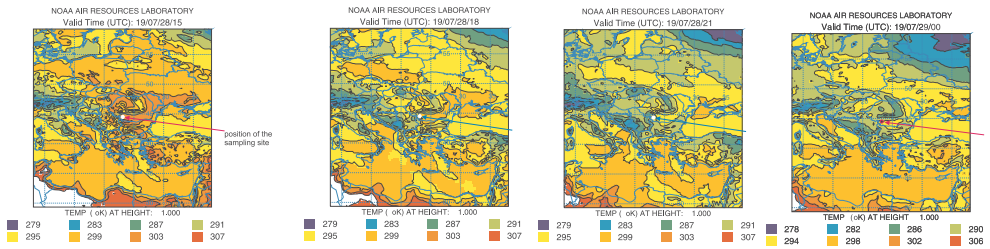


**Figure 7.** A. Regional temperature distribution from 15:00–21:00 UCT, July 28, 2019. Temperatures are given in Kelvin (K). High in feet; B. Cooling related to the storm front is visible from 00:00–15:00 July 29th, ([www.ready.noaa.gov/READYamet.php](http://www.ready.noaa.gov/READYamet.php) and Hysplit).

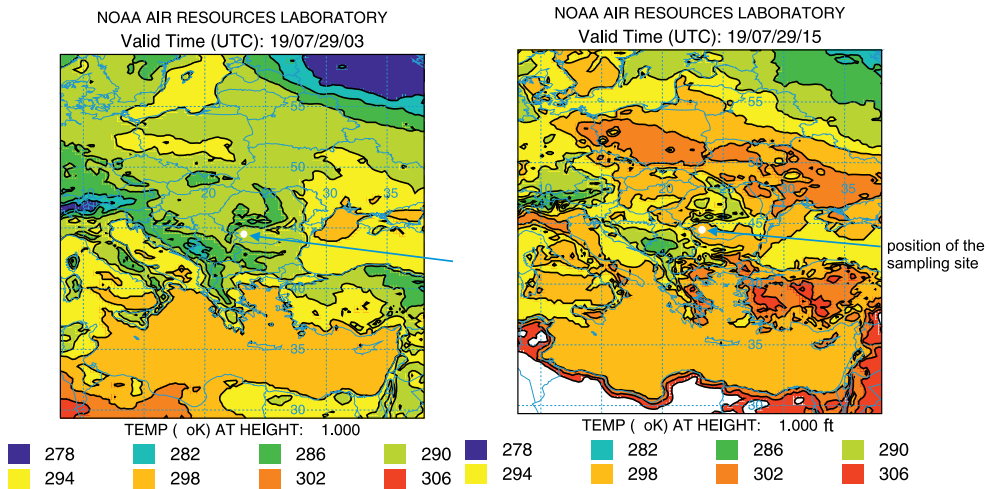


**Figure 7 Continued**

Using Equations (2) and (4), the Rayleigh distillation equation can be used to calculate  $F$ , which represents the fraction of remaining vapour as follows:

$$F = \left( \frac{\alpha_0(\delta_l + 1000)}{\left( \left( \frac{A \cdot 10^3}{T^2} - \frac{B}{T} \right) \left( 1 - e^{-3.3 \left( \frac{T_c - T}{T} \right)} \right) + C \cdot \frac{T_c - T}{T^2} e^{-3.3 \left( \frac{T_c - T}{T} \right)} \right) * (\delta_0 + 1000)} \right)^{\frac{1}{a_m - 1}} \tag{5}$$

### 3. Results

Figure 1A displays the measured values of rainwater  $\delta^{18}\text{O}$  and  $\delta^2\text{H}$  (red diamonds) ranging from  $-0.1$  to  $-7.2$  ‰ and  $-20.3$  to  $-47.8$  ‰, respectively. Figure 1B illustrates

the variations in temperature and rainfall with high temporal isotopic resolution, represented by the 33 samples collected over 456 min (4.6 h). Between 19:50 and 20:31 UCT, temperatures decreased from 21.2–16.5 °C, while rain fluxes fluctuated between multiple maxima and minima, with values ranging from 9 to 238 ml/m<sup>2</sup>/s. The isotope pattern can be described as several superimposed V-shaped sectors, resulting in pronounced local minima and maxima of  $\delta^{18}\text{O}$  and  $\delta^2\text{H}$  values, as shown in Figure 2A. Figure 2B displays the variation of the calculated deuterium excess parameter. The values for the oxygen-18 isotope ratio ( $\delta^{18}\text{O}$ ) and deuterium isotope ratio ( $\delta^2\text{H}$ ) of the rainwater are presented in the biplots (red diamonds and blue squares, respectively) that illustrate the correlation between  $\delta^{18}\text{O}$  and  $\delta^2\text{H}$  and the recorded air temperature (Figures 3 and 4A and B). Figure 2A displays the isotope pattern, which exhibits several periods (I to VIII) indicating the points where the monotony of the isotope composition trend changes. At the onset of the storm, the rain possesses a high isotopic composition. Isotopic variation is mainly due to condensation in sectors where the isotopic composition of the water decreases, such as I to II, III to IV, V to VI, and VII to VIII. Intervals of decreasing values over time alternate with intervals such as II to III, IV to V, VI to VII and VIII until the end of the storm, which are characterised by increasing isotopic values.

#### 4. Discussion

Evaporating rain and surface waters undergo a progressive isotopic enrichment determined by relative humidity of air and temperature [20,21]. The isotopic composition of evaporated water changes along a line with a lower slope than that of the LMWL. This slope can be correlated with the continentality index for Europe, except for regions under the regional climatic influence of the Mediterranean Basin [22]. At low latitudes worldwide, the continentality index may be perturbed at a regional scale, as investigated by for transects across the Andes. The continentality index refers to the  $T_{\text{max}}-T_{\text{min}}$  dependent distribution of rain isotope composition.

For the studied region, the equation of the LMWL was defined through monitoring, measurements, and integration of isotopic data in precipitation, with the determined equation:  $\delta^2\text{H} = 7.58 \cdot \delta^{18}\text{O} + 5.57$  ( $r^2 = 0.9$ ,  $n = 66$ ) (Figure 1). Due to the continuous integration of isotopic data over time, this equation is slightly different from the one published previously [2]. The measured values from the monitored storm define a line (red triangles) that intersects the LMWL. The isotopic composition of the analyzed summer storm waters shifted along an evaporation line described by the equation  $\delta^2\text{H} = 3.56 \cdot \delta^{18}\text{O} - 5.62$  ( $r^2 = 0.68$ ,  $n = 33$ ). The slope of 3.6 is lower than the previously determined slope of 5.6 for the local evaporation line of precipitation (LEL), which intercepts the LMWL at the mean isotopic composition of local springs (yellow circles, Figure 1A). The storm's weighted mean for the values of  $\delta^{18}\text{O}$  and  $\delta^2\text{H}$  are 4.9 and  $-32.5$  ‰, respectively. These values are similar to the mean  $\delta^{18}\text{O}$  and  $\delta^2\text{H}$  values of summer precipitation from June to August, which are  $-5.3$  and  $-36.8$  ‰, respectively.

Intervals II to III, IV to V, VI to VII and VIII until the end of the storm (as shown in Figure 2A) are interpreted as periods of reloading of the storm due to the arrival of a moisture front, as evidenced by the increasing isotopic values. The minimum isotopic values in VIII are reached after the maximum rain intensity, at low temperatures (Figure 2B). As temperatures decrease monotonously, there is no evidence of a warm

front passing through during the whole process. Time series of isotopic values measured during storms have been described as W-shaped isotopic trends [23–26]. The isotopic W-shape trends for the present storm were detected due to detailed sampling of the event and correlation (Figure 2B and A). We propose that the input of multiple rain bands, as described for cyclonic events, may explain this phenomenon.

Figure 2B shows the variations of the deuterium excess ( $d$ ) with time. The deuterium excess was calculated using the equation  $d = \delta^2\text{H} - 8 \cdot \delta^{18}\text{O}$  [19]. The values of  $d$  increase as the rain progresses. At the beginning of the storm, deuterium excess values below 0 ‰ indicate the involvement of recycled continental water in the first rain front. This water evaporated and then condensed during the first cooling front. Even at 100 % relative humidity, the deuterium excess values of waters evaporated from the ocean with isotopic compositions of 0 ‰ are also 0 ‰. During the initial phase of the storm, deuterium excess values were below 0 ‰, suggesting involvement of continental waters with isotopic values lower than those of the oceanic domain (see Figure 2B) [15,27]. The increasing deuterium excess values, along with the arrival of successive rain fronts, may suggest a decrease in moisture during storm formation, ascent and outflow of rain bands, and an increase in the involvement of moisture formed over the Mediterranean Sea. At the end of the event, the deuterium excess values are close to 5 ‰, which is the mean value calculated for the LMWL of the studied region, as shown in Figure 1A.

Figures 3A and 4B display the monthly mean oxygen and hydrogen isotope values of rain from 2011 to 2019 (orange squares) vs. the monthly mean temperature. The storm data (red diamonds) are plotted in the summer sector of the biplots. The scatter in the isotope data can be explained by the temperature variation during the storm period. Examining the summer storm sector reveals that the storm trend displays variations in monotony and isotope values that are not solely linked to a decrease in temperature, but also to an increase in isotope values resulting from the arrival of successive rain fronts.

During cooling, atmospheric air masses undergo rain which causes a change in the fractionation factor between liquid and vapour, which is temperature-dependent (see section 2.4.1).

The calculations presented here are estimative due to the data collection being performed at an altitude of 350 m above sea level, while the condensation of water from the vapour cloud occurs under the cloud surface. It is important to note that the global meteoric water line (GMWL) [28] and the empirical relationships between  $\delta^{18}\text{O}$  and temperature [19,29] are based on data recorded at meteorological stations, rather than from the point of moisture condensation. However, it can be assumed that there was a constant offset between the values considered for the present model and the values where condensation took place. The  $\delta^2\text{H}$  values of vapour were calculated from the measured  $\delta^2\text{H}$  values of rainwater and temperatures using Equation (3) (Figure 5A), and the distributions of the remaining fraction  $F$  of vapour were determined using Equations (2) and (4) (Figure 5B and C). The calculated vapours should be considered as estimates, indicating a general trend of successive incoming fronts.

At the start of the event, the water vapour fraction  $F$  is assumed to be 1 (as shown in Figure 5C).  $F$  is determined by two independent variables: the isotopic composition of the rain and the temperature. The Rayleigh distillation model assumes that, under varying temperatures, a small amount of condensate in equilibrium with the vapours will leave the system as rain. This reduces the vapour fraction  $F$  and exponentially depletes the



system in the heavy isotopes. Figure 5B shows a biplot with the x-axis representing the  $\delta^2\text{H}$  value of rain and the y-axis representing the calculated F (Equation (6)). The plot demonstrates a clear trend and fits a Rayleigh type distribution. F is calculated as a function of two independent variables: air temperature (T) and  $\delta^2\text{H}$  values.

For the analysed storm, the measured  $\delta^2\text{H}$  values of rain do not decrease monotonously. Equation (5) was applied to the isotopic composition from Figure 2A, assuming that vapour masses with a lower degree of 'rain out' and higher isotopic composition enter the system. As a result, F does not decrease monotonously with time as temperature does (Figure 5C). Based on the variable rainfall shown in Figure 1B, we suggest that the storm is successively fed by moisture fronts I, III, V and VII. Each incoming front is plotted on a Rayleigh distribution and marked with an accolade as shown in Figure 5B. According to calculations, approximately 40 % of the water vapour left the system as condensate for the sampled storm (Figure 5B). It is important to note that this is an approximation, as the system was open to the incoming amount. Condensation occurs due to adiabatic expansion and cooling, which brings the air to the dew point. The water vapour lost as condensate lowers the saturation. Rain stops when the cooling can no longer support the dew point and absolute humidity.

Figure 6 shows the moisture displacement track for the thunderstorm that occurred on 28–29 July. The backtracking animation from [www.blitzortung.org/de/historical\\_maps](http://www.blitzortung.org/de/historical_maps) shows that the storm originated in northwestern Spain above the Mediterranean on July 26 and moved across Corsica, Sardinia and Italy. The moist, eastward-flowing air masses formed a counterclockwise belt that moved north across Austria and Hungary. At the same time, the girdle moved eastward and hit the southwestern corner of Romania with a large cell thunderstorm lasting over 6 h, as depicted in Figure 6. The timing of the event, occurring late at night and early in the morning, along with its duration of over 6 h and its synoptic scale, may be indicative of a mesoscale convective complex (MCC) [30]. Figure 7A and B display the temperature distribution at the end of the heat wave on 28 July and the cooling from 29 July, respectively, associated with the array of regional storms.

## 5. Conclusions

By examining a detailed record of stable isotopes, rainfall intensity, and temperature distribution during a 6-hour storm that occurred in the south-western region of Romania following a severe heatwave that struck Europe from 20 to 28 July 2019, the following important points can be highlighted:

- during the storm, deuterium excess data indicate changing moisture sources, starting with recycled continental water and followed by moisture from a marine domain,
- the storm tracks indicate that this event transported moisture from the Mediterranean basin,
- stable isotope values of precipitation along with rain intensity data support the income of distinct rain bands,
- successive rain bands are supported by the stable isotope data plotted on a Rayleigh condensation trend,
- the Rayleigh model output indicates that about 40 % of the moisture was lost as condensate,



- the timing of the event, late at night and early in the morning, its duration of over 6 h and the synoptic scale of the low-pressure cell may be indicative of an MCC.

## Acknowledgements

We are grateful for the comments of two anonymous reviewers; which improved the quality of the paper.

## Disclosure statement

No potential conflict of interest was reported by the author(s).

## ORCID

Ana-Voica Bojar  <http://orcid.org/0000-0002-5266-1754>

## References

- [1] Enciu P. Pliocene and Quaternary of the western part of the Dacian Basin. Stratigraphy and paleogeographical evolution. București: Editura Academiei; 2009.
- [2] Bojar A-V, Halas S, Bojar H-P, et al. Stable isotope hydrology of precipitation and groundwater of a region with high continentality, South Carpathians, Romania. *Carpath J Earth Environ Sci*. 2017;12(2):513–524.
- [3] Bojar A-V, Chmiel S, Bojar H-P, et al. Hydrological system in Quaternary clastic deposits, Mehedinți County, Romania: isotope composition, chemistry and radiocarbon dating. *Geol Soc Spec Publ*. 2021;507:91–105. doi:10.1144/SP507-2020-168
- [4] Bourrié G. Acquisition de la composition chimique des eaux en climat tempéré. Applications aux granites des Vosges et de la Margeride [thesis]. Strasbourg: Université Louis Pasteur; 1978. Français.
- [5] Morrison J, Brockwell T, Merren T, et al. On-line high-precision stable hydrogen isotopic analyses on nanoliter water samples. *Anal Chem*. 2001;73:3570–3575. doi:10.1021/ac001447t
- [6] Werner RA, Brandt WA. Referencing strategies and techniques in stable isotope ratio analysis. *Rapid Commun Mass Spectrom*. 2001;15:501–519. doi:10.1002/rcm.258
- [7] Gröning M, Van Duren M, Andreescu L. Metrological characteristics of the conventional measurement scales for hydrogen and oxygen stable isotope amount ratios: the  $\delta$ -scales. In: Fajgelj A, Belli M, Sansone U, editor. Combining and reporting analytical results. Proceedings of an international workshop on combining and reporting analytical results: the role of traceability and uncertainty for comparing analytical results. Cambridge: Royal Society of Chemistry; 2007. p. 62–72. (Royal Society of Chemistry Special publication; 307).
- [8] Gonfiantini R. Advisory group meeting on stable isotope reference samples for geochemical and hydrochemical investigations. Report to the director general. Vienna: International Atomic Energy Agency; 1984.
- [9] Araguas-Araguas L, Rozanski K. Interlaboratory comparison for deuterium and oxygen-18 analysis of precipitation samples. Report. Vienna: International Atomic Energy Agency; 1995.
- [10] Hut G. Consultants' group meeting on stable isotope reference samples for geochemical and hydrological investigations, report to the director general. Vienna: International Atomic Energy Agency; 1987.
- [11] Koziat J. Isotope ratio mass spectrometric method for the on-line determination of oxygen-18 in organic matter. *J Mass Spectrom*. 1997;32:103–108. doi:10.1002/(SICI)1096-9888(199701)32:1<103::AID-JMS463>3.0.CO;2-9

- [12] Horita J, Ueda A, Mizukami K, et al. Automatic  $\delta\text{D}$  and  $\delta^{18}\text{O}$  analyses of multi-water samples using  $\text{H}_2$ - and  $\text{CO}_2$ -water equilibration methods with a common equilibration set-up. *Int J Radiat Appl Instrum Appl Radiat Isot.* 1989;40:801–805. doi:10.1016/0883-2889(89)90100-7
- [13] McCarthy KT, Pichler T, Price RE. Geochemistry of Champagne Hot Springs shallow hydrothermal vent field and associated sediments, Dominica, Lesser Antilles. *Chem Geol.* 2005;224:55–68. doi:10.1016/j.chemgeo.2005.07.014
- [14] Wassenaar LI, Terzer-Wassmuth S, Douence C, et al. Seeking excellence: an evaluation of 235 international laboratories conducting water isotope analyses by isotope-ratio and laser-absorption spectrometry. *Rapid Commun Mass Spectrom.* 2018;32:393–406. doi:10.1002/rcm.8052
- [15] Majoube M. Fractionnement en oxygene-18 et en deuterium entre l'eau et sa vapeur. *J Chim Phys.* 1971;68:1423–1436. Français. doi:10.1051/jcp/1971681423
- [16] Kakiuchi M, Matsuo S. Direct measurements of D/H and  $^{18}\text{O}/^{16}\text{O}$  fractionation factors between vapor and liquid water in the temperature range from 10°C. *Geochem J.* 1979;13:307–311. doi:10.2343/geochemj.13.307
- [17] Horita J, Wesolowski DJ. Liquid–vapor fractionation of oxygen and hydrogen isotopes of water from the freezing to the critical temperature. *Geochim Cosmochim Acta.* 1994;58:3425–3437. doi:10.1016/0016-7037(94)90096-5
- [18] Halas S. About isotope equilibrium between liquid and vapor phases. *Isot Environ Health Stud.* 2008;44:129–135. doi:10.1080/10256010802066125
- [19] Dansgaard W. Stable isotopes in precipitation. *Tellus.* 1964;16:436–468. doi:10.1111/j.2153-3490.1964.tb00181.x
- [20] Gonfiantini R. Environmental isotopes in lake studies. In: Fritz P, Fontes J-C, editor. *Handbook of environmental isotope geochemistry. Vol. 2, the terrestrial environment.* Amsterdam: Elsevier; 1986. p. 113–168.
- [21] Gibson JJ, Birks SJ, Yi Y. Stable isotope mass balance of lakes: a contemporary perspective. *Quat Sci Rev.* 2016;131:316–328. doi:10.1016/j.quascirev.2015.04.013
- [22] Lécuyer C, Bojar A-V, Daux V, et al. Geographic variations in the slope of the  $\delta^2\text{H}$ – $\delta^{18}\text{O}$  meteoric water line over Europe: a record of increasing continentality. In: Bojar A-V, Pelc A, Lécuyer C, editor. *Stable isotope studies of the water cycle and terrestrial environments.* London: Geological Society; 2021. p. 5–17. (Geological Society Special Publications; 507).
- [23] Aemisegger F, Pfahl S, Sodemann H, et al. Deuterium excess as a proxy for continental moisture recycling and plant transpiration. *Atmos Chem Phys.* 2014;14(8):4029–4054. doi:10.5194/acp-14-4029-2014
- [24] Rindsberger M, Jaffe S, Rahamim S, et al. Patterns of the isotopic composition of precipitation in time and space: data from the Israeli storm water collection program. *Tellus.* 2022;42B:263–271. doi:10.3402/tellusb.v42i3.15218
- [25] Celle-Jeanton H, Gonfiantini R, Travi Y, et al. Oxygen-18 variations of rainwater during precipitation: application of the Rayleigh model to selected rainfalls in Southern France. *J Hydrol.* 2004;289:165–177. doi:10.1016/j.jhydrol.2003.11.017
- [26] Li J, Tao T, Pang Z, et al. Identification of different moisture sources through isotopic monitoring during a storm event. *J. Hydrometeorol.* 2015;16(4):1918–1927. doi:10.1175/JHM-D-15-0005.1
- [27] Zhao L, Wang L, Liu X, et al. The patterns and implications of diurnal variations in the d-excess of plant water, shallow soil water and air moisture. *Hydrol Earth Syst Sci.* 2014;18(10):4129–4151. doi:10.5194/hess-18-4129-2014
- [28] Craig H. Isotopic variations in meteoric waters. *Science.* 1961;133:1702–1703. doi:10.1126/science.133.3465.1702
- [29] Fricke H, O'Neil J. The correlation between  $^{18}\text{O}/^{16}\text{O}$  ratios of meteoric water and surface temperature: Its use in investigating terrestrial climate change over geologic time. *Earth Planet Sci Lett.* 1999;170(3):181–196. doi:10.1016/S0012-821X(99)00105-3
- [30] Feidas H. Study of a mesoscale convective complex over Balkans with Meteosat data. In: Helmis C, Nastos P, editor. *Advances in meteorology, climatology and atmospheric physics.* Berlin, Heidelberg: Springer; 2013. p. 79–85. (Springer Atmospheric Sciences).